

High resolution spectroscopy of nearby AGN

J.S. Kaastra¹

SRON National Institute for Space Research, Sorbonnelaan 2, 3584 CA Utrecht, The Netherlands

Abstract. In this paper the potential of high resolution spectroscopy of nearby AGN with XEUS is discussed. The focus is upon the energy resolution that is needed in order to disentangle the different spectral components. It is shown that there is an urgent need for high spectral resolution, and that a spectral resolution of 1 eV, if possible, leads to a significant increase in diagnostic power as compared to 2 eV resolution.

1. Introduction

Since the launch of Chandra and XMM-Newton, with their high resolution spectrometers, our insight into the astrophysics of Active Galactic Nuclei (AGN) has changed dramatically. It is now possible to study in detail the geometry, dynamics and physical state of the warm absorber, as well as the underlying continuum spectrum, including the exciting possibility of relativistic emission lines. While with XMM-Newton and Chandra high resolution, high signal-to-noise ratio spectra of the brightest (and in general the nearest) AGN can be taken, the large resolving power and effective area of XEUS will allow us to study AGN spectra out to large redshifts or low intrinsic luminosities. It will also allow time-resolved spectroscopy of the most rapidly varying AGN. A detailed understanding of the astrophysics and spectral signatures of the nearest AGN is an absolute requirement in order to understand the properties of the most distant AGN that will be observed by XEUS, which will have much noisier spectra. In this contribution spectral simulations are presented that show the potential and limitations of AGN spectroscopy with XEUS.

2. Spectral simulations

I have performed a set of spectral simulations of a bright Seyfert 1 galaxy as will be observed with XEUS. For the effective area of the instrument I took the area as foreseen in the final configuration of XEUS (taken from the XEUS web page).

For the spectral resolution a parameterization of what currently is thought to be feasible was taken: a constant full width at half maximum (FWHM) of 2 eV below 1 keV, 10 eV above 14 keV and in between a linear interpolation. A spectral response matrix was generated with a Gaussian energy resolution consistent with the FWHM and effective area mentioned above. All spectral simulations were done using the SPEX package version 2.0 (Kaastra et al. 2002b).

For the Seyfert 1 spectrum I took a prototype of a bright and nearby AGN: NGC 5548. This Seyfert 1 galaxy was the first to be observed at high spectral resolution (Kaastra et al. 2000). It has a moderate redshift of 0.017, and a low Galactic column density. The spectral model I used is described below, and is based upon the modeling of the Chandra LETGS data (Kaastra et al. 2002a) for most energies, supplemented by the Fe-K line emission as modeled by Yaqoob et al. (2001) based upon the Chandra HETGS data.

The ingredients of our spectral model are:

- a power law continuum
- a modified blackbody spectrum, describing the accretion disk continuum at low energies
- a warm absorber, consisting of three ionization and five velocity components, with a range of -160 to -1060 km/s outflow velocity
- narrow forbidden emission lines from O VII and Ne IX
- a narrow Fe-K line component at 6.4 keV

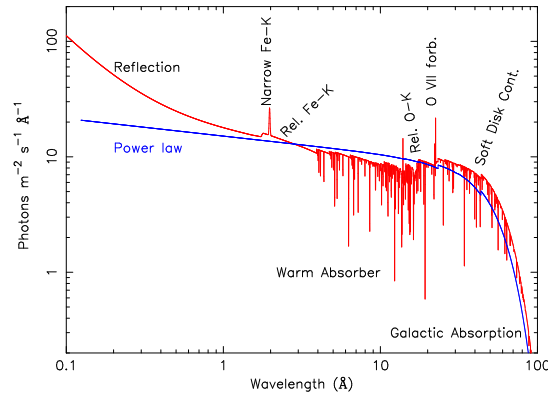


Fig. 1. Model spectrum at high spectral resolution for NGC 5548, with the different spectral components as indicated. The blue line indicates the underlying power law component. Note that nowhere in the spectrum the total model spectrum looks similar to the underlying power law!

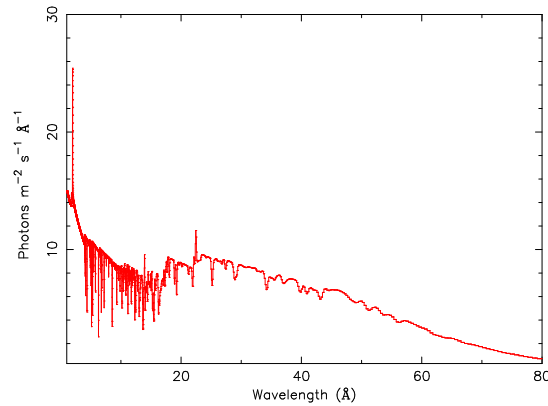


Fig. 2. Model spectrum for NGC 5548, folded with the energy resolution of XEUS.

- a relativistic Fe-K line
- weak relativistic O VIII and N VII Ly α lines
- a reflection component at high energies

The model photon spectrum corresponding to the above model, as would be seen with very high energy resolution, is shown in Fig. 1. The model spectrum, but now folded with the XEUS spectral resolution, is shown in Fig. 2. Note that nowhere in the model spectrum there exists an energy range where the spectrum agrees fully with the underlying power law component. At high energies there is the excess of the reflection component, around 6 keV the broad iron line component causes excess flux, then at lower energies the warm absorber reduces the observed flux, followed by excess emission at the lowest energies, due to emission from the accretion disk, including the modified blackbody as well as any possible relativistic Ly α lines from oxygen and nitrogen.

Thus, in order to derive the underlying AGN continuum or any of the other spectral components, the spectrum must be fitted over the entire wavelength range, taking into account all contributions. It is also seen that due to the fact that XEUS will use non-dispersive X-ray detectors, the spectral resolution at low energies is relatively poor and not all the spectral lines can be resolved (compare Fig. 1 with Fig. 2). I come back later to this point.

3. Finding relativistic lines

The presence of relativistic emission lines from O VIII and N VII Ly α has been discussed first by Branduardi-Raymont et al. (2001) based upon XMM-Newton RGS observations of the narrow line Seyfert 1 galaxies MCG -6-30-15 and Mrk 766. In these two galaxies the relativistic lines are very strong, although another group disputes this result (Lee et al. 2001). The flux level in both sources is quite strong, so statistics is not really the problem, but the debate depends heavily upon disentangling the different spectral components. A stronger warm absorber would produce deeper oxygen absorption edges, and hence would leave less room for a relativistic oxygen emission line. But in order to get a reliable

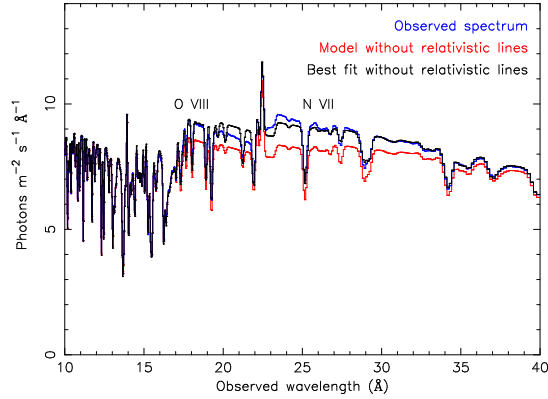


Fig. 3. Model spectrum of NGC 5548 with the XEUS resolution near the region of the relativistic oxygen and nitrogen lines. The blue curve is the simulated spectrum for 40 ks integration time (error bars are very small and invisible); the red curve is the same model spectrum but with the relativistic lines left out; the black curve is the best fit model for a model that does not take into account the relativistic lines.

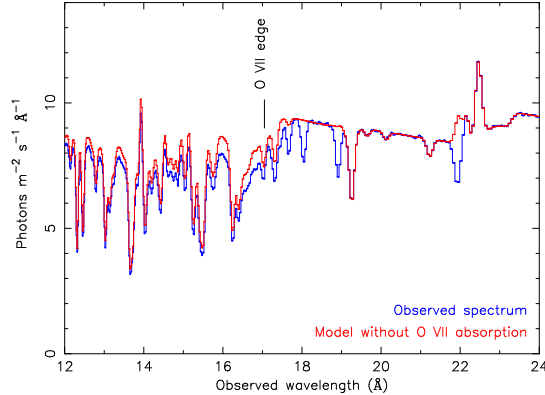


Fig. 4. Blue line: model spectrum of NGC 5548 with the energy resolution of XEUS. Red curve: same model, but with the O VII column density put to zero.

estimate of the depth of the oxygen absorption edges, which are strongly contaminated by several other absorption lines and edges, a detailed modeling of the absorption lines is needed, and for that purpose high spectral resolution is a necessary condition.

In NGC 5548 the relativistic lines are much weaker, as is shown in Fig. 3. It is seen from this figure that the maximum amplitude of these lines is at most $\sim 15\%$, around 24 \AA . It is also seen that when the relativistic lines are not taken into account, the resulting spectral fit agrees quite well with the observed spectrum. The differences in the continuum are less than a few percent, in a region where very likely also instrumental neutral oxygen edges will be present. This therefore poses severe constraints on the calibration of the effective area, which must be better than a percent over broad energy ranges.

A way out is of course by looking to the spectral lines in order to constrain the depth of the absorption edges. But for that purpose the highest possible spectral resolution is needed.

4. Complexity of the warm absorber

The complexity of the warm absorber is illustrated in Fig. 4. From the difference of the model with and without the O VII it is seen that in the observed photon spectrum the K-edge of O VII cannot be distinguished, due to strong blending by several weak inner shell iron lines (see below). The apparent "edge" is rather smooth, and moreover from the jump in the continuum between 16 \AA and 18 \AA it is not possible to measure directly the depth of the oxygen edge: the effective depth of the "edge" is significantly deeper than just the contribution from O VII alone. Again, high resolution is needed in order to estimate accurately the depth of the O VII edge, based upon the equivalent width ratios of the absorption lines from the same ion. Due to blending, which is in particular important at low spectral resolution,

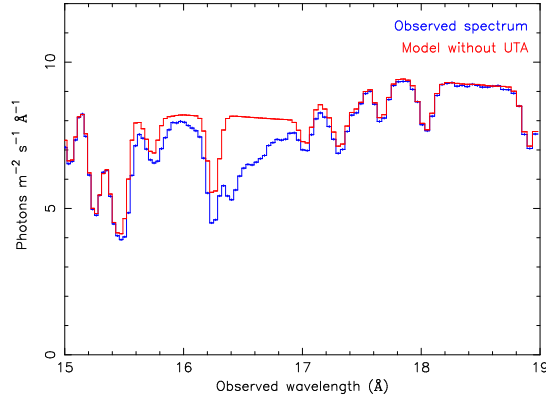


Fig. 5. Blue curve: model spectrum of NGC 5548 with the energy resolution of XEUS; red curve: same model, but with the column densities of the Fe-M ions put to zero.

but which cannot always be avoided even at high energy resolution due to the finite velocity width of the absorption complexes, it is important to observe several lines of the same ion.

One of the reasons for the complexity of the spectrum near the O VII edge is demonstrated in Fig. 5. In this range of the spectrum there are many weak inner-shell absorption lines due to lowly ionized iron (in our model Fe IX–Fe XVI). These lines were first recognized by Sako et al. (2001) in their analysis of the quasar IRAS 13349+2438. It is seen that these lines constitute a broad, unresolved blend. They are very important from a diagnostic point of view, since they measure directly the strength of the less ionized material in the warm absorber, for ionization parameters that yield otherwise only spectral lines mostly in the inaccessible (E)UV range.

5. Why high spectral resolution is needed

High spectral resolution is important in order to determine the spectral line parameters of the warm absorber and thereby the continuum spectrum. This is illustrated in Fig. 6. This figure simulates the transmission of a slab composed of pure O VIII. For other ions the effects illustrated in this figure are qualitatively similar. The model spectrum has been convolved with the currently adopted XEUS spectral resolution of 2 eV.

For the reference model (O VIII column 10^{22} m^{-2} , velocity dispersion $\sigma_v = 250 \text{ km/s}$, outflow velocity $v = 0 \text{ km/s}$ and covering factor $f_{\text{cov}} = 1$), the Ly α , Ly β and Ly γ lines are strongly saturated, and hence doubling the column density does not change these line profiles significantly. Note that for this velocity dispersion, the intrinsic width of the Ly α line is about 1.2 eV and hence unresolved with the 2 eV instrumental resolution. In many Seyfert galaxies the intrinsic line width can be even smaller than the value used here. The difference in column density can only be seen for the higher order lines (Ly δ and higher) but these lines start becoming blended with each other (in the model, I took all lines up to $n = 10$ into account). And of course the difference in column density can be seen near the continuum edge, but as I have shown before the continuum edge is often very hard to measure due to severe contamination by various spectral lines and line blends, and due to the unknown underlying continuum spectrum.

Measuring the intrinsic velocity broadening σ_v appears at a first glance more promising. By doubling σ_v to 500 km/s, the Ly α and Ly β lines become significantly deeper, while the higher lines of the series become less deep, because they are smeared out. The Ly α and Ly β lines become deeper because their (equivalent) width doubles and now becomes comparable to the instrumental resolution. However it should be noted that the intensity at the deepest point of the *observed* Ly α line is still not zero, despite the fact that the line core in the original *model* spectrum is completely black. This is due to the limited spectral resolution of the instrument.

This, in fact, causes that the apparent sensitivity for changes in σ_v is partially an illusion, as is illustrated with the light blue curve, where the same enhanced σ_v of 500 km/s was adopted but now with a covering factor of only 75 %. Now the observed line profiles are very similar to the original reference model with σ_v of 250 km/s and full covering factor! The difference would be most clearly visible in the continuum edge, where the transmission differs by 25 %, but as was pointed out before these continuum edges are difficult to measure accurately.

Finally, Fig. 6 also shows the sensitivity to measure outflow velocities. Outflow velocities of 500 km/s can be measured by using line centroiding. For the Ly α line, this velocity corresponds to a 1 eV shift, so can be easily detected. Note however that in many AGN the absorption lines are composed of several velocity components, which are separated by velocity differences on the hundred km/s velocity scale. Each velocity component may have its own

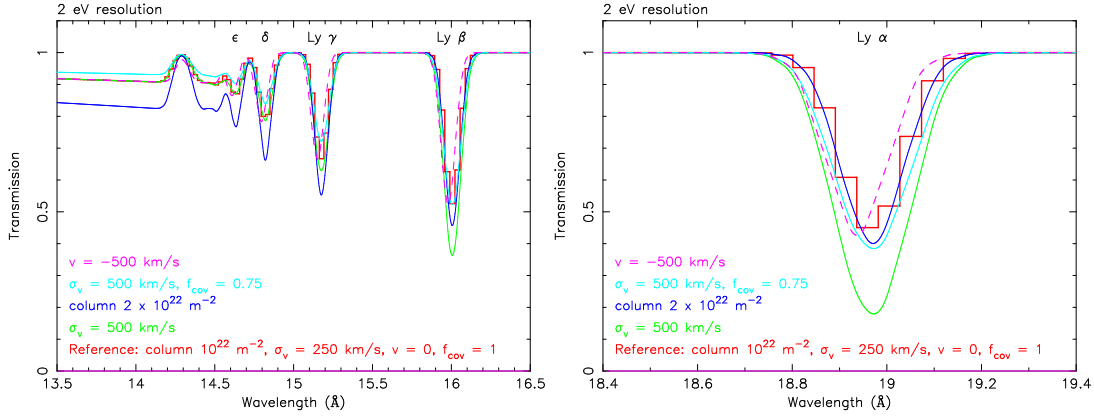


Fig. 6. Different models for the transmission of a slab composed of pure O VIII. The model spectra are folded through an instrument with an energy resolution of 2 eV (as is used for the present XEUS simulations). Right panel: the Ly α line; Left panel: the higher Lyman lines and the O VIII edge. The reference model (red curve) has an O VIII column of 10^{22} m^{-2} , a velocity dispersion of 250 km/s, an outflow velocity of 0 km/s and a covering factor of unity. The other curves have the same parameters except the ones indicated in the caption.

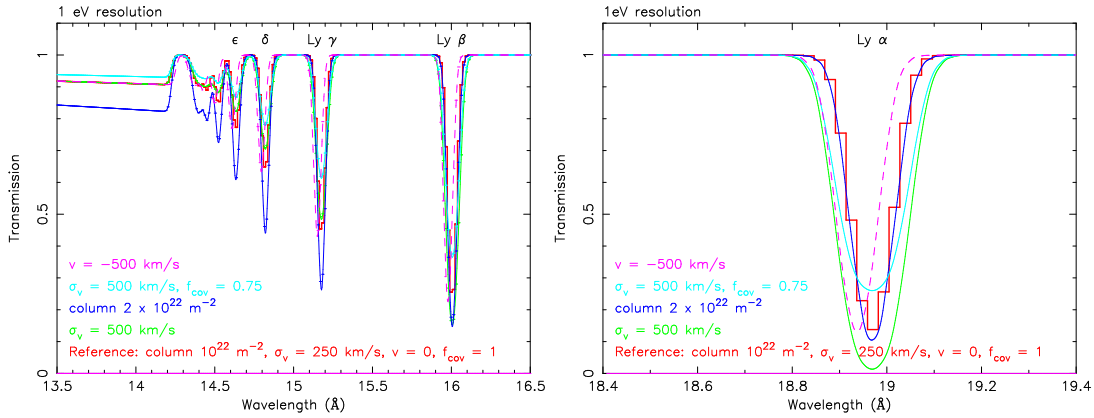


Fig. 7. Same as Fig. 6, but instead a 1 eV instrumental resolution.

ionization structure, hence what is observed as a single broad absorption line is actually composed of a complex set of line components, hence any gain in spectral resolution is extremely useful.

Needless to say that for cosmologically redshifted AGN the situation becomes even more problematic, due to the fact that the lines shift to lower energies with poorer instrumental resolution.

Therefore I have also made a set of calculations for the line profiles with a spectral resolution of 1 eV instead of 2 eV (Fig. 7). Such a factor of two improvement of the spectral resolution does not seem impossible from a technical point of view, in particular if the spectral resolution is optimized for these lower energies (below 2 keV). Improving the spectral resolution by a factor of two also enhances the sensitivity for weak lines with a factor of two, without even increasing the effective area! Comparing both figures, it is seen that the observed lines now appear much deeper, and hence the accurate measurement of covering factors can be done more easily. The differences between the various cases shown in the figure are much more pronounced.

Apart from a significant improvement in the determination of the intrinsic line widths and centroids, a major advantage of a higher spectral resolution is also that contamination due to blending by lines from other ions can be severely reduced. Note that our above simulation was done for a slab consisting of pure O VIII, but in reality the spectrum is composed of a mixture of absorption lines from many ions with different velocity and ionization structure.

This is illustrated in Fig. 8, where I compare the original model spectrum with the model spectrum folded through 1 and 2 eV instrumental resolution. It is clear that for both instrumental resolutions the velocity fine structure of the absorption lines cannot be resolved. This is currently a great advantage of the UV band, where instruments like FUSE or the STIS instrument of HST are able to provide very high spectral energy resolution (down to the 10 km/s scale). In fact, STIS observations served as the basis for our velocity model applied in this figure. Nevertheless, it is

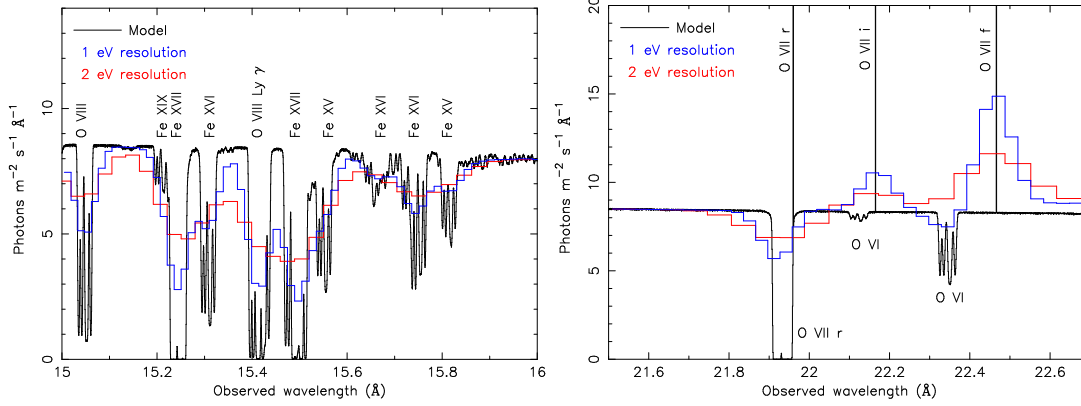


Fig. 8. Model spectrum at high resolution (black line), convolved with an instrumental resolution of 1 eV (blue line) and 2 eV (red line). Left panel: region near 15 Å containing O VIII, Fe XVII and other important diagnostic lines; right panel: region near the O VII triplet.

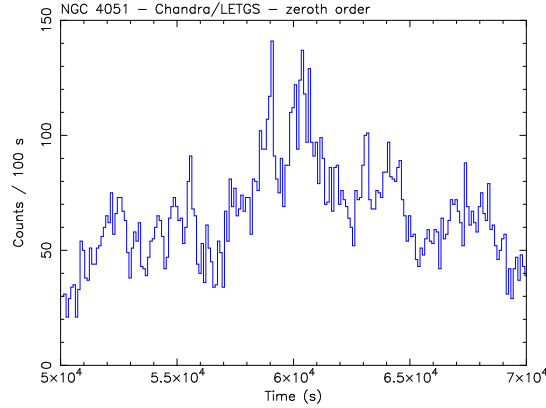


Fig. 9. Chandra LETGS light curve in first order of NGC 4051. Time bins: 100 s.

evident from this figure that a 1 eV spectral resolution is a significant improvement over a 2 eV spectral resolution. For example, the O VIII Ly γ line at 15.18 Å (observed here at 15.4 Å due to the cosmological redshift) and the Fe XVII line at 15.27 Å (observed at 15.5 Å) are not separated with 2 eV resolution but can be distinguished clearly at 1 eV resolution. With 2 eV resolution, it would be difficult to see if it is a blend of two narrower components, or for example a single broad, red/blueshifted line. The same holds for separating the Fe XV and Fe XVI lines around 15.8 Å.

Also near the O VII triplet a gain in spectral resolution is very important. With 2 eV resolution the intercombination line of O VII cannot be measured, and also the important O VI inner shell absorption line, observed at 22.35 Å is only visible with 1 eV resolution, since it is so close to the strong forbidden emission line. This O VI line, as well as similar inner shell absorption lines from O I – O V at slightly longer wavelengths, are very important, as they cover a broad range of ionization parameter with ions from the same chemical element, thus avoiding modeling difficulties due to unknown elemental abundances. Although the inner shell Fe-lines (the UTA mentioned before) around 15–17 Å also cover this range of ionization parameter, the analysis of these lines is much more complicated due to the strong blending, while the oxygen lines are in a relatively clean part of the spectrum (the 21–24 Å range).

6. Time variability

The large effective area of XEUS makes it ideal to study rapid time variability. For the high luminosity AGN variability typically occurs on time scales of days or longer, so for those sources variability studies are limited by the finite exposure time available for each target. However, for low luminosity AGN the intrinsic variability time scales can be much faster. An example is given in Fig. 9. This AGN shows rapid variability, down to the time scale of 100 s.

With the current generation of grating spectrometers it is not possible to obtain high quality spectra with such a short integration time on the minute time scale. However with the effective area of XEUS this is not a problem. This is illustrated in Fig. 10. XEUS is able to obtain high S/N spectra for bright Seyfert 1 galaxies in just 100 s

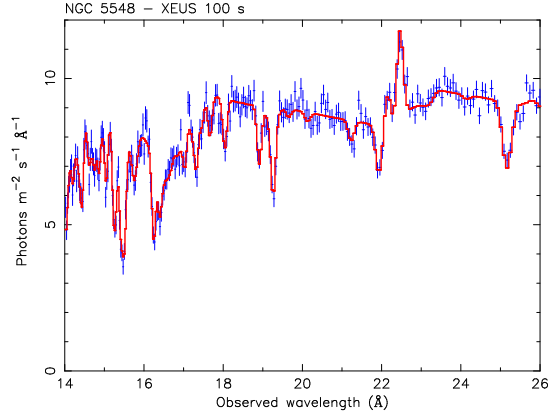


Fig. 10. Simulated spectrum for NGC 5548 with a 100 s integration time.

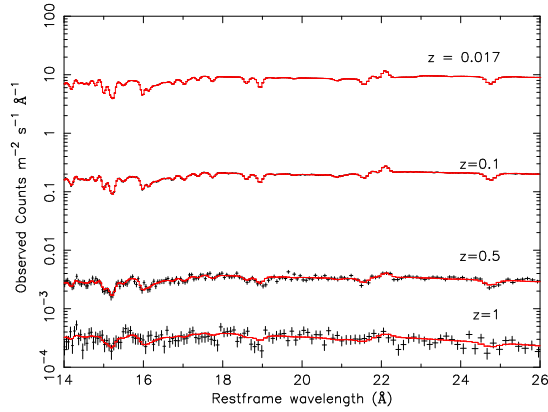


Fig. 11. Simulated spectra for NGC 5548 with 40 ks exposure time, for redshifts of 0.017, 0.1, 0.5 and 1 (from top to bottom). The y-axis represents the fluxed spectrum in the *observers* frame, however for easy of comparison the x-axis has been shifted to the rest frame wavelength. For the lowest redshift, the error bars on the spectrum are barely visible.

integration time. This allows a study of the intrinsic variations of the accretion disk spectrum on this time scale. For example, if an AGN has strong relativistic oxygen and nitrogen lines, and it varies rapidly on this time scale, all kinds of reverberation methods can be applied and the geometry of the innermost part of the accretion disk can be well constrained.

The large effective area of XEUS is of course not only excellent for high time resolution observations of bright and nearby AGN, it also will allow to obtain good spectra of distant AGN. This is illustrated in Fig. 11. In that figure NGC 5548 is put at redshifts of 0.017 (its true redshift), 0.1, 0.5 and 1. Good quality spectra within a reasonable net exposure time (half a day) is possible up to $z = 0.5$. At $z = 1$, the spectrum becomes too noisy at the highest spectral resolution, and also due to the cosmological redshift the spectral resolution degrades, making it harder to disentangle the narrow spectral components. For example, for $z = 1$, the O VII triplet cannot be resolved, both due to the low source flux and the factor of 2 poorer spectral resolution, as compared to the case of $z = 0.017$. Of course, for higher luminosity AGN good spectra can be obtained out to larger redshifts.

Acknowledgements. SRON is supported financially by NWO, the Netherlands Organization for Scientific Research.

References

- Branduardi-Raymont, G., Sako, M., Kahn, S.M., et al., 2001, *A&A* 365, L140
 Kaastra, J.S., Mewe, R., Liedahl, D.A., Komossa, S., & Brinkman, A.C., 2000, *A&A* 354, L83
 Kaastra, J.S., Steenbrugge, K.C., Raassen, A.J.J., et al., 2002a, *A&A* 386, 427
 Kaastra, J.S., Mewe, R., & Raassen, A.J.J. 2002b, in *New Visions of the X-ray Universe in the XMM-Newton and Chandra Era*, ed. F.A. Jansen, ESA, in press
 Lee, J.C., Ogle, P.M., Canizares, C.R., et al., 2001, *ApJ* 554, L13

Sako, M., Kahn, S.M., Behar, E., et al. 2001, A&A 365, L168

Yaqoob, T., George, I.M., Nandra, K., et al., 2001, ApJ 546, 759